Atmos. Chem. Phys. Discuss., 10, 1135–1166, 2010
www.atmos-chem-phys-discuss.net/10/1135/2010/

Atmospheric Chemistry and Physics Discussions

This discussion paper is/has been under review for the journal Atmospheric Chemistry and Physics (ACP). Please refer to the corresponding final paper in ACP if available.

Cirrus clouds triggered by radiation, a multiscale phenomenon

F. Fusina and P. Spichtinger

ETH Zurich, Institute for Atmospheric and Climatic Science, Universitaetstrasse 16, 8092 Zurich, Switzerland

Received: 22 October 2009 – Accepted: 20 December 2009 – Published: 18 January 2010

Correspondence to: F. Fusina (fabian.fusina@env.ethz.ch)

Published by Copernicus Publications on behalf of the European Geosciences Union.

Abstract

In this study, the influence of radiative cooling and small eddies on cirrus formation is investigated. For this purpose the non-hydrostatic, anelastic model EULAG is used with a recently developed and validated ice microphysics scheme (Spichtinger and Gierens, 2009a). Additionally, we implemented a fast radiation transfer code (Fu et al., 1998). Using idealized profiles with high ice supersaturations up to 144% and weakly stable stratifications with Brunt-Vaisala frequencies down to $0.018\,s^{-1}$ within a supersaturated layer, the influence of radiation on the formation of cirrus clouds is remarkable. Due to the radiative cooling at the top of the ice supersaturated layer with cooling rates down to $-3.5\,K/d$, the stability inside the ice supersaturated layer decreases with time. During destabilization, small eddies induced by Gaussian temperature fluctuations start to grow and trigger first nucleation. These first nucleation events then induce the growth of convective cells due to the radiative destabilization. The effects of increasing the local relative humidity by cooling due to radiation and adiabatic lifting lead to the formation of a cirrus cloud with IWC up to $33\,mg/m^3$ and mean optical depths up to 0.36. In a more stable environment, radiative cooling is not strong enough to destabilize the supersaturated layer within 8 h; no nucleation occurs in this case.

Overall triggering of cirrus clouds via radiation works only if the supersaturated layer is destabilized by radiative cooling such that small eddies can grow in amplitude and finally initialize ice nucleation. Both processes on different scales, small-scale eddies and large-scale radiative cooling are necessary.

1 Introduction

The existence of cloud-free air masses that are supersaturated with respect to (over) ice in the upper troposphere or lowermost stratosphere is known since long time. More than 60 years ago, Glückauf (1945) obtained values for relative humidity with respect to ice (RHi) up to 160% (over Southern England). The fact, that high ice supersaturations

can occur in the upper troposphere has been neglected for many years and has often been termed as errors. During the last two decades the existence of air masses in the status of supersaturation was proven by many measurements with a variety of different measurement techniques (e.g., Jensen et al., 1998; Vay et al., 2000; Ovarlez et al., 2000; Kraemer et al., 2009). These measurements are consistent with theoretical considerations, that ice crystals form at very high supersaturations, whereas the exact freezing threshold depends on the nucleation mechanism (homogeneous freezing of solution droplets or heterogeneous nucleation, see e.g., Koop et al., 2000; De Mott et al., 2003, respectively). For homogeneous nucleation, which is probably the dominant mechanism for forming ice crystals at low temperatures ($T < -38\,^{\circ}\mathrm{C}$) relative humidities in the range 140 to 170% RHi, depending on temperature (Koop et al., 2000), are required.

The properties and global distributions of ice supersaturated regions (ISSRs) were discovered during the last years (e.g., Spichtinger et al., 2003a,b; Gettelman et al., 2006). They occur 20 to 30% of the time in cloud free air masses of the upper troposphere over the North Atlantic. Because of the large horizontal extensions of ISSRs with mean path lengths of about 150 km and some rare events with extension of few thousands of kilometers (Gierens and Spichtinger, 2000) there is a substantial amount of cloud free air masses with enhanced water vapor content. However, only few parametrizations exist for the physical correct formation of cirrus clouds (from ISSRs) driven by synoptic scale dynamics (CAM3, see Lin et al., 2007; ECHAM5, see Kärcher and Lohmann, 2002). The impact of meso- and small-scale motions is not regarded explicitly, although some approximations are used to obtain meso-scale motions (Kärcher and Lohmann, 2002). The radiative impact of ISSRs (with RHi up to 130%) has been investigated by Fusina et al. (2007). These regions of enhanced water vapor can reduce the total outgoing longwave radiation by more than $1\mathrm{W/m}^2$ and imply a significant cooling at their upper boundary (i.e. due to thermal emission).

In a stable stratified atmosphere, these diabatic heating-rates are too small to influence the local dynamics crucially. But if potential stability of the environment is weak or

neutral, radiative cooling can decrease the Brunt-Vaisala frequency to a critical value, and following to an increased amplitude and extend of preexisting small scale motions. The combination of the locally amplified vertical velocity and the radiative cooling can trigger the first nucleation. Regions with weak stratification (i.e. small vertical gradients of potential temperature) have been observed in the upper troposphere, using radiosonde data obtained over the meteorological observatory in Lindenberg, Germany. In these regions dynamical instabilities could also occur: The Miles theorem describes that a stable atmosphere is given with a Richardson number $Ri > 0.25$,

$$Ri = \frac{N^2}{\left(\frac{\partial u}{\partial z}\right)^2}, \quad \text{using} \quad N^2 = \frac{g}{\theta}\frac{\partial \theta}{\partial z} \tag{1}$$

where N denotes the Brunt-Vaisala frequency. Moderate and strong windshears are often observed in the upper troposphere, as described by Birner (2006).

In this study, we investigate the possibility of cirrus cloud formation, due to radiative cooling in weakly stable layers within the upper troposphere. Sensitivity studies are carried out for the most important initial parameters as potential stability, windshear and RHi within the ISSR. The main purpose is to investigate the sensitivity on environmental conditions, for which radiative cooling (a large scale process) at the top of an ISSR can destabilize the stratification. During the destabilization, the amplitude of preexisting small scale eddies increase and trigger cloud formation. Only the superposition of effects on different scales (i.e. large-scale radiative cooling and small scale motions) can finally lead to cirrus formation. The main properties of possibly formed cirrus clouds are investigated, as ice water content (IWC), ice crystal number density (N), cloud life time and their impact on the radiation. For this purpose, the non-hydrostatic anelastic model EuLag (Eulerian, semi-Lagrangian Model) is used (e.g., Prusa et al., 2008), using a two stream radiation transfer code (Fu, 1996; Fu et al., 1998) and an ice microphysics scheme (Spichtinger and Gierens, 2009a).

The paper is organized as follows: In the next section, the model is described briefly. In Sect. 3 we define the experimental setup for the reference simulations. In the

following Sect. 4, results of the reference and sensitivity simulations are presented. We end with discussions and conclusions.

2 Model description

As a basic dynamical model, the anelastic nonhydrostatic model EULAG is used (see Prusa et al., 2008). The dry anelastic equations solved in the model are presented in Smolarkiewicz and Margolin (1997).

2.1 Ice physics

A recently developed bulk ice microphysic scheme is used, which can treat an arbitrary number of ice classes. Theses ice classes are distinguished due to their formation mechanism (e.g. heterogeneously vs. homogeneously formed ice). The following processes for cold cirrus clouds are parameterized: nucleation (homogeneous), deposition (growth, evaporation) and sedimentation (Spichtinger and Gierens, 2009a). It provides a consistent double moment scheme with terminal velocities for ice number and mass concentration. Aggregation is not yet implemented in the microphysics scheme. However, aggregation is of less importance for the cold temperature regime ($T<-38\,^{\circ}$C) and/or for moderate vertical velocities (Kajikawa and Heymsfield, 1989).

For the parametrization of homogeneous freezing of aqueous solution droplets, sulfuric acid solution droplets are assumed as a background aerosol, using a lognormal distribution for the H_2SO_4 droplet size (geometric standard deviation σ_r=1.4, geometric mode radius r_m=25 nm, total number concentration 300 cm^{-3}). The freezing rates are calculated using a temperature based parametrization, based on water activity (see Koop et al., 2000). We use a modified Koenig ansatz (Koenig, 1971) to parameterize the diffusional growth or evaporation for small ice crystals, including corrections for the kinetic grow regime and ventilation, respectively. For all simulations in this study, only homogeneous nucleation is taken into account. For details of the model, the more interested reader is referred to Spichtinger and Gierens (2009a).

2.2 Radiation transfer model

A two stream radiation transfer code, i.e. a representation of forward and backward streams, has been implemented into the EuLag model. It contains 6 bands in the solar and 12 bands in the thermal infrared regime. For a detailed description, the interested reader is referred to Fu (1996) for the shortwave and to Fu et al. (1998) for the longwave parametrization, respectively.

The required parameters from ice microphysics are ice water content (IWC) and effective radius, which is derived following Slingo (1989), Dobbie et al. (1999) and Fu (1996). In the microphysical model ice crystals are assumed to be small hexagonal columns. The ice crystal size is lognormally distributed with a geometric standard deviation of σ_L=1.5. The effective radius is calculated as described in Fusina et al. (2007) under the assumption of randomly oriented columns (Ebert and Curry, 1992).

The radiation transfer code uses following constant trace gas concentrations: CO_2: 330 ppmv; CH_4: 1.6 ppmv; N_2O: 0.28 ppmv, respectively. The ozone profile depends on altitude including the stratospheric ozone layer. The model domain of the radiation transfer code has a maximum altitude of L_{zr}=50 km, which is not necessarily equivalent to the top level of the EULAG model (L_z). The vertical resolution within the EULAG model domain is set by the model setup. If $L_{zr}>L_z$ (this is the case for our simulations), the vertical resolution of the additional layers exceeding the EULAG model domain is set to 1 km, the water vapor mixing ratio is set to $q_v=10^{-11}$ kg/kg, the pressure profile is interpolated using the US standard atmosphere; the temperature profile is built using a constant lapse rate up to a final temperature of T(50 km)=275 K (according to the US standard atmosphere, COESA, 1976), respectively. The solar zenith angle is set to 60° and the solar surface albedo is 0.3. The infrared surface emissivity is assumed to be 1.

3 Experimental setup

For the simulations, an idealized framework is used, including a 2-D model domain with a horizontal extent of L_x=12.8 km and a vertical extent of L_z=15 km for dynamics and ice microphysics, respectively. An ISSR is placed between lb=9500 m and ub=10500 m with a constant relative humidity over ice of 140%, which fully occupies the whole horizontal extent of this layer. RHi below and above the ISSR is set to 60% and 5%, respectively (see Fig. 2, left panel). Using a grid resolution of dx=100 m and dz=50 m, in the horizontal and the vertical, respectively, the domain is discretized with $nx \times nz$=128×301 grid points.

A constant-stratification ambient profile of potential temperature, as described by Clark and Farley (1984), is used with a surface temperature T=293.15 K and a Brunt-Vaisala frequency N=0.0094 s^{-1}. Within the layer between 9250 m and 10 750 m altitude, the stability of the stratification is decreased to a constant vertical gradient of the potential temperature of $\partial\theta/\partial z$=0.4 K/km (which corresponds to a Brunt-Vaisala frequency N=0.0035 s^{-1}). The tropopause is placed at an altitude of 12 000 m (see Fig. 2 middle). The stability above the tropopause is set to N=0.02 s^{-1}. The profile of the horizontal velocity contains a constant wind below and above and a weak windshear of $\partial u/\partial z$=1×10^{-3} s^{-1} (for the reference case) within the ISSR (Fig. 2, right panel):

$$u(z) = \begin{cases} 1 & \text{for } 0 \le z < lb, \\ 1 + du_z \cdot (z - lb) & \text{for } lb \le z \le ub, \\ 1 + du_z \cdot (ub - lb) & \text{for } lb < z. \end{cases} \quad (2)$$

The initial potential temperature field is distributed by a Gaussian noise with standard deviation σ_T = 0.01 K. All simulations run for a total time of 8 h with 1 s increments for the dynamics, optional 0.1 s increments for the ice physics in case of homogeneous nucleation and 10 s increments for the radiation, respectively. We assume a calm troposphere, i.e. no vertical wind in our small 2-D domain.

4 Results

4.1 Reference case

At the beginning of the reference case simulation, only radiative processes (emission and absorption of LW radiation) can change dynamical and microphysical properties in the domain. The obtained heating rates (see Fig. 3) have an impact on two major characteristics within the ISSR. First, the temperature decrease (strongest at the top) tends to increase RHi with a rate of ∼+1% per hour (see Fig. 4c). Second, the stability of the stratification decreases with time, reaching its lowest neutral/unstable state at t=200 min (see Fig. 4a), where the first unstable grid cells (i.e. with a negative squared Brunt-Vaisala frequency) occur at t=150 min. Within this first 200 min, small eddies (induced by initial temperature fluctuations) are growing due to the destabilization and start to lift up air parcels, temporally increasing their RHi. Patterns within the vertically averaged turbulent kinetic energy (TKE) underline the formation and growth of this small cells. However, the vertical velocities are not increasing significantly, before the stratification becomes unstable, but the amplitude of the temperature deviations is increasing slightly.

After t=200 min, the eddies start to grow rapidly in size (favored by the unstable environment) and therefore, the first air parcels reach the threshold of homogeneous nucleation of 156% (see Fig. 4c). This effect happens only in several small isolated cells, surrounded by downwelling regions. Latent heat release due to the growth of the ice crystals amplifies the motions inside the ISSR, increasing the vertical velocity from its preliminary w_{max}=±0.03 m/s up to w_{max}=±0.5 m/s, forming convective cells. The formed cirrus cloud is persistent over the rest of the simulation time, containing ice crystal number concentrations up to N=300 L^{-1} and a maximum mean ice water path of $\overline{IWP}$=2.95 g/m^2 (averaged over all columns). The peak with the highest ice water content corresponds to a local maximum of the vertical velocity. The whole time evolution for $\overline{IWP}$ is showed in Fig. 4d.

At the time of maximum $\overline{\text{IWP}}$, an optical depth of $\bar{\tau}$=0.1 is derived. $\bar{\tau}$ is averaged over all columns, observing a peak-value of τ=0.36, which is significantly higher than the mean value due to the patchiness of the cloud. Due to the high supersaturation inside the layer, the formed ice crystals grow rapidly and start to sediment. During the downward motion, they continue to grow and deplete water vapor, reducing the RHi in the lower part of the ISSR. In the down welling regions, some entrainment of very dry air from above of the ISSR can be observed, making the 2-D field of RHi more patchy than before. Within the upper part of the ISSR, on the top of the upwelling regions, the RHi remains at the homogeneous freezing threshold for a longer time, contineously forming new ice crystals (Fig. 4, t=360 min).

4.2 Variation of potential stability

The initial vertical gradient of the potential temperature θ is changed within the ISSR. For a small windshear, as it is used in the reference case and in this set of sensitivity simulations, this value represents the stability because of high Richardson numbers. Cases with stronger windshear will be discussed in the next section. A set of value is chosen as: $\partial\theta/\partial z$ = 0.1/0.2/0.3/0.4/0.5/0.6/0.8 K/km (corresponding Brunt-Vaisala frequencies N=0.0018/0.0025/0.003/0.0035/0.0039/0.0043/0.005 s^{-1}, respectively). These values have been compared with radiosonde records obtained from routine measurements over the meteorological observatory Lindenberg, Germany (see e.g., Spichtinger et al., 2003a). The dataset covers the time period from 1 February 2000 to 30 April 2001 with measurements every 6 h (i.e. 00:00, 06:00, 12:00, 18:00 UTC). 14.7% of all profiles show a layer of at least 500 m thickness, containing a potential stability between 0.1 and 0.8 K/km (5% for stabilities lower than 0.4 K/km; reference case). 3.26% of all profiles contain the same stability, but within a layer of at least 1 km thickness (0.64% for stabilities lower than 0.4 K/km, i.e. reference case). These cases are filtered for temperatures lower than 235 K for comparison in potential cirrus regions. It follows that the values used in this sensitivity study are in the range of atmospheric relevance.

All cases of this sensitivity simulation fulfill the Miles theorem for shear stability (i.e. Ri>0.25). All other simulation parameters are equal to the reference case.

When we reduce the vertical gradient of the potential temperature of the reference case (0.4 K/km) to $\partial\theta/\partial z$=0.2 K/km, the maximum obtained amount of $\overline{\text{IWP}}$ increases from $\overline{\text{IWP}}$=3×10^{-3} kg/m^2 to $\overline{\text{IWP}}$=6.8×10^{-3} kg/m^2. This peak value appears 100min earlier, than in the reference case and corresponds to the moment of maximum kinetic energy within the ISSR (i.e. the vertical wind speeds are strongest; see Fig. 6b). One can conclude, that in simulations with a lower stability inside the ISSR, nucleation occurs earlier than in the reference case due to two reasons. First, the amplitude of the temperature variation inside the small eddies is larger due to the lower stability. Second, and more important, the destabilization of the layer due to radiation is faster, starting at lower Brunt-Vaisala frequencies. The obtained amount of $\overline{\text{IWP}}$ is higher for cases with weaker initial stabilities; Fig. 6a). The largest $\overline{\text{IWP}}$=8.9×10^{-3} kg/m^2 (with a maximum value of IWC=33 mg/m^3) can be observed for the simulation with the weakest initial potential stability, 170 min after initialization. The main reason for the higher IWP are the higher vertical velocities obtained in the simulations with weaker initial stability, resulting in higher ice crystal amounts (Fig. 7). In the simulation with the weakest stability (0.1 K/km), vertical updrafts up to w=1.6 m/s are observed in some isolated cells. If the initial stability is reduced further, then convective cells can be generated already due to the initial temperature perturbations and the role of the radiation in the cloud building process is no more dominant (i.e. the superposition of these two effects, radiation and small eddies, is no longer required). For higher initial stabilities the destabilization event takes more time. For all simulations with a stronger stability than the reference case, the simulation time of 480 min is not sufficient to deplete the whole supersaturation inside the layer. In this cases, layer-clouds are formed in the upper part of the ISSR. If the initial stability exceeds the threshold of 0.8 K/km, no nucleation occurs within the 8 h simulation time.

4.3 Variation of wind shear

In a second set of sensitivity simulations, the impact of different strengths of wind shear is determined while the thermal stratification is set to the reference value of $\partial\theta/\partial z$=0.4 K/km. We use values of $\partial u/\partial z$=0/1/2/4/6/8×10^{-3} s^{-1} in the altitude range 9500≤z≤10 500 m (see Fig. 8a). The chosen values are weak, but in the range of observations in the upper troposphere (see, e.g., the statistics presented by Birner, 2006). For the strongest wind shear $\partial u/\partial z$=8×10^{-3} s^{-1}, the initial Richardson Number Ri=0.19<0.25 is below the threshold for shear instability. In this case, we expect the formation of Kelvin-Helmholtz instabilities. Values of wind shear above this threshold are not for interest for this study, because the mixing effect of shear instability would superimpose with the destabilization effect of radiative cooling in a unpredictable amount. All other simulation parameters are equal to the reference case.

For this set of sensitivity simulations, the highest $\overline{\text{IWP}}$=4.15×10^{-3} kg/m^2 was observed for zero windshear. In this scenario, the formation and evolution of the isolated convective cells is not affected by windshear. So, the cells have a larger vertical extent than in the cases with windshear. Related to the statistics in Birner (2006), it has to be considered that for the mid-latitudes windshear-free scenarios are very unlikely for cirrus altitudes. Increasing the windshear to $\partial u/\partial z$=2×10^{-3} s^{-1} reduces the vertical extent of the upwelling regions and the vertical updraft velocity inside. The cells start to tilt with height. Due to the increased mixing inside the ISSR, less regions with RHi close to the homogeneous threshold are observed. This leads to a restrained nucleation, whereby the number of ice crystals N decreases. Increasing the windshear more will amplify this effects, leading to lower IWPs (see Fig. 8b). For windshears of $\partial u/\partial z$≥4×10^{-3} s^{-1}, shear instability is generated with time. This leads to more turbulent motions inside the ISSR and results in stronger vertical velocities followed by a increased homogeneous nucleation rate. For the case with the highest windshear of $\partial u/\partial z$≥8×10^{-3} s^{-1}, a pronounced Kelvin-Helmholtz instability develops after t=440 min, containing vertical updraft velocities of w>2 m/s. The cirrus clouds formed

by turbulence due to shear instabilities even appear, when the radiation code is disabled. Due to that, they are not of interest for this study. It can be concluded that, after the destabilization of the stratification due to radiative cooling, isolated eddies are a key feature of cirrus clouds triggered by radiation, supported by the latent heat release after the first nucleation event. Their evolution and persistence is suppressed by stronger wind-shears. Windshear can also block the destabilization of the layer with the highest radiative cooling rate, by mixing it with the surrounding air. But this happens only for values close to the threshold for shear instability (Ri≤0.25).

4.4 Variation of RHi

A third set of sensitivity simulations uses different amounts of water vapor inside the ISSR. By increasing the RHi, the gap to the homogeneous freezing thresholds is decreased, so an earlier nucleation can be expected. Decreasing the RHi leads to the opposite effect. The used values for RHi are 132/136/140/144%, respectively. Windshear and thermal stability are set to the values in the reference case ($\partial u/\partial z$=10^{-3} s^{-1}, N=0.0035 s^{-1}).

For simulations with a maximum RHi lower than in the reference case, it takes more time to reach the homogeneous freezing threshold (i.e. due to cooling from emission and adiabatic lifting). On the other hand, the radiative cooling inside the ISSR is a function of the RHi (i.e. the water vapor mixing ratio) as discussed in Fusina et al. (2007). Thus, for lower RHi values at the same temperature, the cooling rates decrease. This results in a slower destabilization of the upper part of the ISSR. The differences between the updraft velocities are small, a significant change in the numbers of ice crystals can not be observed between the different simulations. It follows that instead of the ice crystals number, their size increases, due to the enhanced water-vapor content, increasing the terminal velocities (i.e. their fall speed). This can modulate the cirrus life time, as larger crystals fall faster down to subsaturated regions and sublimate.

For the simulation with RHi=144%, the nucleation starts 15 min earlier than in the reference case, obtaining a maximum $\overline{\text{IWP}}$ that is 30% higher. A comparison of the

$\overline{\text{IWP}}$ between the different sensitivity simulations is given in Fig. 9. In the simulations with RHi=136/140/144%, a second nucleation peak at the end of the simulation can be observed. This nucleation event is possibly triggered by the latent heat release during the earlier ice crystal forming, superimposed with destabilization due to radiative cooling. If the initial RHi is reduced to less than 132%, the cooling will again get weaker and no destabilization (i.e. formation of an updraft) and due to that, no nucleation occurs during the simulation time of 8 h. If the initial RHi is increased to 150% or more, the small scale motions due to the initial temperature fluctuations are strong enough to trigger nucleation without any previous change in the local stability due to radiative cooling.

4.5 Variation of upper RHi gradient

In a next step, beside the variation of the total amount of water vapor, the influence of the water vapor gradient at the top of the ISSR on the local heating rates is discussed. Radiosonde profiles show a variety of different shapes of the RHi profile in the upper troposphere. In Fig. 10, two different radiosonde profiles with different water vapor gradients are shown. We use the same setup as in the reference case simulation (maximum RHi=140%) and increase the vertical distance in which the RHi decreases from its maximum value down to RHi=5% near the tropopause, using following values: dz=250/500/750/1000/1500 m, where dz=250 m stands for the reference case (see Fig. 11a).

In Fig. 11b, the heating rates for the different RHi gradients can be seen. It becomes obvious, that for lower gradients, the cooling area is distributed over a larger vertical layer than for stronger gradients. Therefore, the maximum cooling peak is lower, resulting in a weaker destabilization of the upper layer. Thus, only the profiles with the strongest two initial RHi-gradients have been able to trigger the described cirrus formation mechanism within the simulation time of 8 h (assuming all other parameters to be equal to the reference case). This might be a point, that restricts this kind of cloud

formation process. A strong descent of RHi at the upper boundary of the ISSR is strictly required for destabilization due to radiative cooling. One example for a sufficient strong RHi gradient is shown in Fig. 10.

4.6 Variation of temperature

Another way to change the water vapor content within the ISSR is to vary the vertical temperature profile. Using constant initial values for RHi in the ISSR implies that for a increasing temperature, the water vapor mixing ratio will increase too. This influences the local heating rates and due to radiation also the destabilization of the stratification. The destabilization due to radiation is faster for profiles with higher environmental temperatures and the formed cirrus has a larger IWC. However, the general sensitivity of higher H_2O content in the upper troposphere is shown in Sect. 4.4.

4.7 Radiative impact

The variation of the potential stability has the biggest influence on the radiative properties of the formed cirrus cloud. Increasing the initial $\partial\theta/\partial z$ from 0.1 to 0.8 K/km (i.e. N=0.0018 to 0.005 s^{-1}), the maximum value of the mean optical depth (i.e. averaged for all columns for every time step) decreases from $\overline{\tau}$=0.36 to 0.05 (see Fig. 12a–c). It has to be considered, that this is a mean value over the whole domain and the values for single columns can be considerably larger (i.e. the largest optical depth for a single column can be observed in case of the smallest potential stability: τ_{max}=0.82). The smallest changes of τ can be observed for the sensitivity study of changing initial RHi ($\overline{\tau}$=0.14 to 0.08). For all cases, the calculated total outgoing radiation fluxes (the sum of shortwave and longwave radiation) decrease by a certain amount after the cloud formation, i.e. the difference between the absorbed and emitted longwave radiation inside the cloud exceeds the amount of reflected shortwave radiation at the cloud top (warming scenario, see Fusina et al., 2007).

5 Conclusions

The nonhydrostatic, anelastic model EULAG (Prusa et al., 2008) was used with a recently developed and validated ice microphysic scheme (Spichtinger and Gierens, 2009a) and an additionally implemented fast radiation transfer code (Fu et al., 1998) to investigate the influence of a superposition of radiative cooling and small eddies on cirrus formation. For that purpose, idealized profiles with high supersaturations up to 144% RHi and weak thermal stability have been used. The focus is on the multiscale aspect of cirrus formation superimposing large scale (i.e. radiative cooling) with small scale (i.e. small eddies) effects. Only the combination of these effects could lead to significant cloud formation. The results can be summarized as follows: Destabilization due to radiative cooling can lead to amplification of small scale eddies, which can act as an initial cloud forming factor. A sensitivity study for following parameters has been done: static and dynamic stability and the RHi within the ISSR. The values of this key factors should be between 0.1 and 0.8 K/km for the thermal stability (i.e. the vertical gradient of the potential temperature), 132 to 144% RHi and there should occur no shear instability ($Ri > 0.25$).

From our investigations we could answer some questions concerning the formation of cirrus clouds due to radiative cooling:

1. Cooling due to thermal emission at the top of an ISSR can destabilize a initial weak stable profile within several hours (depending on the initial stability and RHi).
2. During destabilization, the amplitude of initial small eddies increases and leads to the first nucleation of ice crystals. Supported by the following latent heat release, vertical updraft velocities up to 1.6 m/s can be provided.
3. Within the first 8 h, cirrus clouds are formed with mean ice water paths up to 8.9×10^{-3} kg/m^2 and ice crystal number densities up to N=350 L^{-1}.

4. In sensitivity studies it was shown, that increasing the initial potential stability would delay the first nucleation event up to several hours and decrease the strength of the nucleation event, as we can see for $\overline{\text{IWP}}$ and N. Increasing the initial windshear would lead to smaller cells, and therefore to fewer nucleation. Increasing the RHi within the ISSR amplifies the thermal emission and shortens the time to the first nucleation event, but it has only a marginal effect on the vertical velocities. This will lead to cirrus clouds with larger $\overline{\text{IWP}}$.
5. To obtain sufficient radiative cooling at the top of the ISSR, a steep decrease of RHi is required.

Using a simple phase-diagram (Fig. 13) we can explain the sensitivity due to certain parameters. If the initial RHi is lower than the boundary a, the radiative cooling would be to weak to destabilize the stratification, if it is to high (boundary c), the random motions due to initial temperature fluctuations would be strong enough, to trigger a cloud before the profile gets unstable. If the stability (static or dynamic) gets to weak (boundary b), updrafts can be triggered spontaneously due to initial small-scale motions or induced shear-instability, if it gets too strong (boundary d), the radiative cooling is again not strong enough to destabilize the profile within an certain time (8 h for this simulations). At least for conditions near the boundary (b), it is very hard to distinguish, which of the observed effects (e.g. destabilization due to radiative cooling, shear-instability, small-scale eddies) actually is the most important. It has to be considered, that we have always a superposition of different cloud-controlling effects on different scales. It must be noted here, that without radiative cooling at the top of the ISSR, there would be no cloud formation for all simulations within 8 h. This implies, that other cloud building mechanisms like frontal lifting or orographic effects (i.e. gravity waves) (e.g., Spichtinger and Gierens, 2009b; Joos et al., 2009) should not occur during the simulation time.

Acknowledgements. We thank the European Centre for Medium-Range Weather Forecasts for computing time (special project SPCHCLAI "Cloud aerosol interactions") and Andreas Doernbrack, Ulrike Lohmann and Thomas Peter for fruitful discussions. This work contributes to the project "Impact of dynamics on cirrus clouds" (Grant: 200021-117700) supported by the Swiss National Science Foundation (SNSF).

References

Birner, T.: Fine-scale structure of the extratropical tropopause region, J. Geophys. Res., 111, D04104, doi:10.1029/2005JD006301, 2006. 1138, 1145

Clark, T. and Farley, R.: Severe downslope wind- storm calculations in two and three spatial dimensions using anelastic interactive grid nesting: a possible mechanism for gustiness, J. Atmos. Sci., 41, 329–350, 1984. 1141

COESA: US Commission/Stand Atmosphere (Compiler), Natl. Oceanic & Atmospheric Admin (Collaborator), Natl. Aeronautics & Space Admin (Collaborator), United States Air Force (Collaborator), US Standard Atmosphere, NOAA, NASA, USAF, NOAA Document S/T 76-1562, 1st edn., 1976. 1140

Dobbie, J. S., Li, J. N., and Chylek, P.: Two- and four-stream optical properties for water clouds andsolar wavelengths, J. Geophys. Res., 104, 2067–2079, 1999. 1140

Ebert, E. E. and Curry, J. A.: A parametrization of ice cloud optical properties for climate models, J. Geophys. Res., 97, 3831–3836, 1992. 1140

Fu, Q. A.: An accurate parameterization of the solar radiative prop- erties of cirrus clouds for climate models, J. Climate, 9, 2058–2082, 1996. 1138, 1140

Fu, Q., Yang, P., and Sun, W. B.: An accurate parameterization of the infrared radiative properties of cirrus clouds for climate models, J. Climate, 11, 2223–2237, 1998. 1136, 1138, 1140, 1149

Fusina, F., Spichtinger, P., and Lohmann, U.: Impact of ice supersaturated regions and thin cirrus on radiation in the midlatitudes, J. Geophys. Res., 112, D24S14, 2007. 1137, 1140, 1146, 1148

Gettelman, A., Walden, V. P., Miloshevich, L. M., Roth, W. L., and Halter, B.: Relative humidity over Antarctica from radiosondes, satellites, and a general circulation model, J. Geophys. Res., 111, D09S13, doi:10.1029/2005JD006636, 2006. 1137

Gierens, K. and Spichtinger, P.: On the size distribution of ice-supersaturated regions in the upper troposphere and lowermost stratosphere, Ann. Geophys., 18, 499–504, 2000, http://www.ann-geophys.net/18/499/2000/. 1137

Glückauf, E.: Notes on upper air hygrometry-II: on the humidity in the stratosphere, Q. J. Roy. Meteor. Soc., 71, 110–112, 1945. 1136

Jensen, E. J., Toon, O. B., Tabazadeh, A., Sachse, G. W., Anderson, B. E., Chan, K. R., Twohy, C. W., Gandrud, B., Aulenbach, S. M., Heymsfield, A., Hallett, J., and Gary, B.: Ice nucleation processes in upper tropospheric wave-clouds during SUCCESS, Geophys. Res. Lett., 25, 1363–1366, 1998. 1137

Joos, H., Spichtinger, P., and Lohmann, U.: Orographic cirrus in a future climate, Atmos. Chem. Phys., 9, 7825–7845, 2009, http://www.atmos-chem-phys.net/9/7825/2009/. 1150

Kärcher, B. and Lohmann, U.: A parameterization of cirrus cloud formation: homogeneous freezing of supercooled aerosols, J. Geophys. Res., 107(D2), 4010, doi:10.1029/2001JD000470, 2002. 1137

Kajikawa, M. and Heymsfield, A.: Aggregation of ice crystals, J. Atmos. Sci., 46, 3108–3121, 1989. 1139

Koenig, L.: Numerical modeling of ice deposition, J. Atmos. Sci., 28, 226–237, 1971. 1139

Koop, T., Luo, B., Tsias, A., and Peter, T.: Water activity as the determinant for homogeneous ice nucleation in aqueous solutions, Nature 406, 611–614, 2000. 1137, 1139

Krämer, M., Schiller, C., Afchine, A., Bauer, R., Gensch, I., Mangold, A., Schlicht, S., Spelten, N., Sitnikov, N., Borrmann, S., de Reus, M., and Spichtinger, P.: Ice supersaturations and cirrus cloud crystal numbers, Atmos. Chem. Phys., 9, 3505–3522, 2009, http://www.atmos-chem-phys.net/9/3505/2009/. 1137

Ovarlez, J., van Velthoven, P., Sachse, G., Vay, S., Schlager, H., and Ovarlez, H.: Comparison of water vapor measurements from POLINAT 2 with ECMWF analyses in high humidity conditions, J. Geophys. Res., 105, 3737–3744, 2000. 1137

Prusa, J. M., Smolarkiewicz, P., and Wyszogrodzki, A.: EULAG, a computational model for multiscale flows, Comput. Fluids, 37(9), 1193–1207, doi:10.1016/j.compfluid.2007.12.001, 2008. 1138, 1139, 1149

Slingo, A.: A GCM parameterization for the shortwave radiative properties of water clouds, J. Atmos. Sci., 46, 1419–1427, 1989. 1140

Smolarkiewicz, P. and Margolin, L.: On forward- in-time differencing for fluids: an Eulerian/Semi-Lagrangian non-hydrostatic model for stratified flows, Atmos. Ocean, 35, 127–152, 1997. 1139

Spichtinger, P., Gierens, K., Leiterer, U., and Dier, H.: Ice supersaturation in the tropopause region over Lindenberg, Germany, Meteorol. Z., 12, 143–156, 2003a. 1137, 1143

Spichtinger, P., Gierens, K., and Read, W.: The global distribution of ice supersaturated regions as seen by the microwave limb sounder, Q. J. Roy. Meteor. Soc., 129, 3391–3410, 2003b. 1137

Spichtinger, P. and Gierens, K. M.: Modelling of cirrus clouds – Part 1a: Model description and validation, Atmos. Chem. Phys., 9, 685–706, 2009, http://www.atmos-chem-phys.net/9/685/2009/. 1136, 1138, 1139, 1149

Spichtinger, P. and Gierens, K. M.: Modelling of cirrus clouds – Part 1b: Structuring cirrus clouds by dynamics, Atmos. Chem. Phys., 9, 707–719, 2009, http://www.atmos-chem-phys.net/9/707/2009/. 1150

Vay, S. A., Anderson, B. E., Jensen, E. J., Sachse, G. W., Ovarlez, J., Gregory, G. L., Nolf, S. R., Podolske, J. R., Slate, T. A., and Sorenson, C. E.: Tropospheric water vapor measurements over the North Atlantic during the Subsonic Assessment Ozone and Nitrogen Oxide Experiment (SONEX), J. Geophys. Res., 105, 3745–3756, 2000. 1137

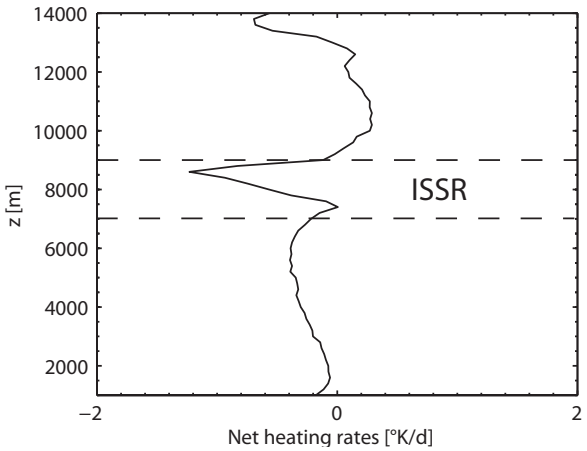

Fig. 1. Heating-rates [K/d] of an ISSR with RHi=130% due to emission and absorption of radiation.

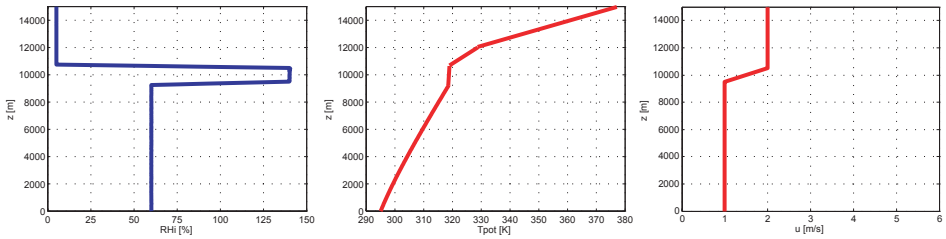

Fig. 2. Vertical profiles used for the reference simulation. Left: RHi profile; middle: potential temperature profile; right: horizontal velocity profile.

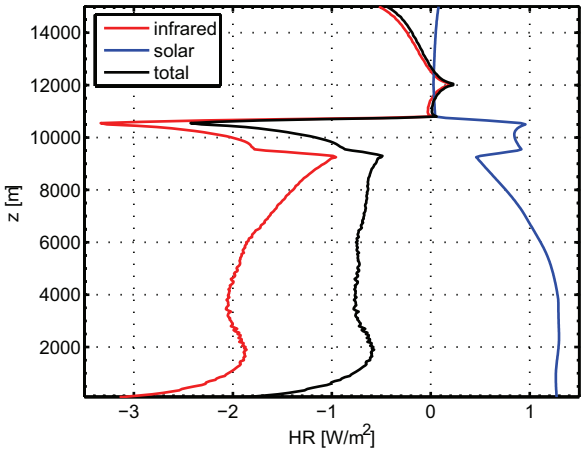

Fig. 3. Vertical radiative heating rates (split into solar, infrared and total) at the initial time step, containing an ISSR with maximum RHi of 140%.

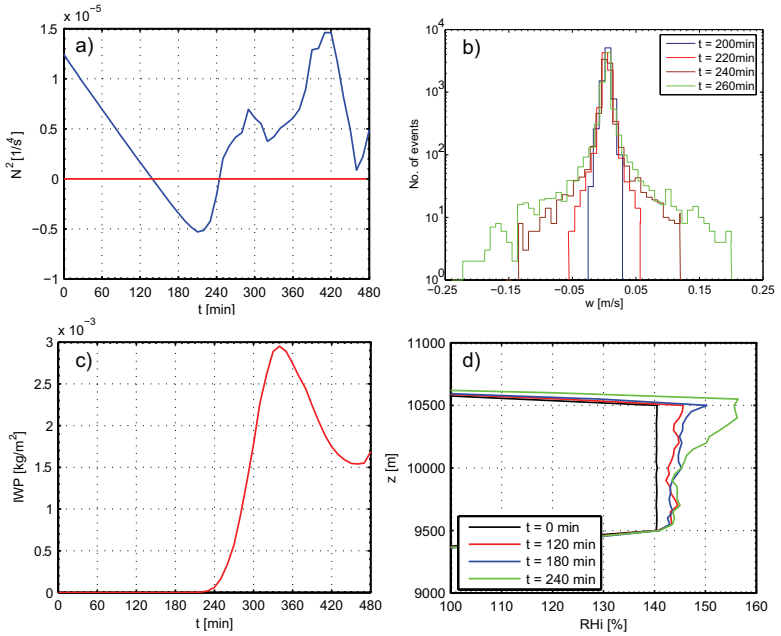

Fig. 4. **(a)** Time evolution of horizontal mean of the squared Brunt-Vaisala frequency at z=10 500 m (altitude of maximum cooling); **(b)** histogram: vertical velocity for 4 different timesteps (200/220/240/260 min); **(c)** time evolution of mean ice water path (IWP); **(d)** maximum RHi for 4 different timesteps (0/120/180/240 min).

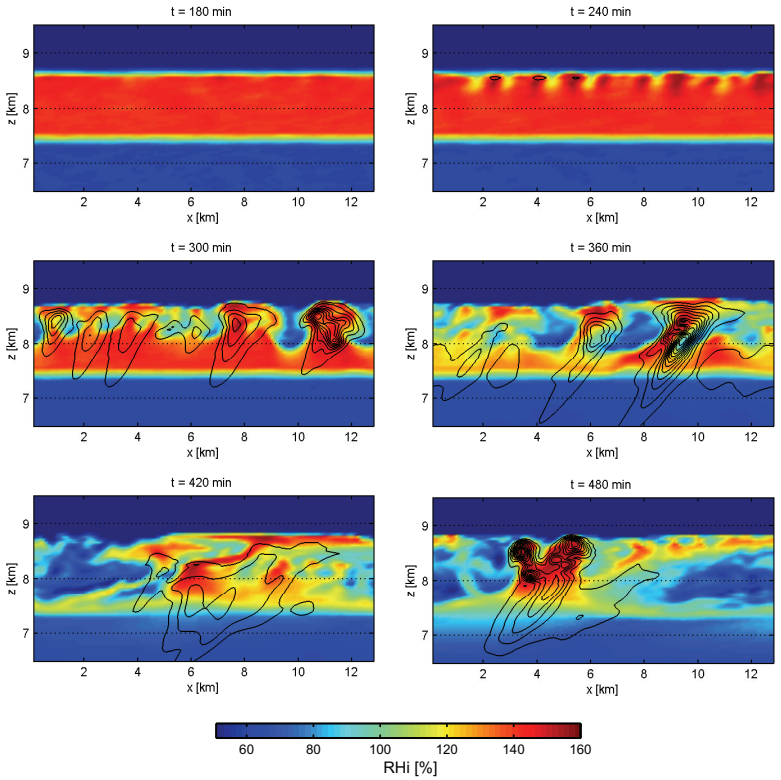

Fig. 5. Cirrus cloud formation in the reference simulation – colors indicate RHi in %; contour lines represent IWC [10^{-6} kg/m^3] increments. Time evolution: 1. destabilization at ISSR top, first nucleation. 2. Developement of the cloud/convective cells. 3. Entrainment.

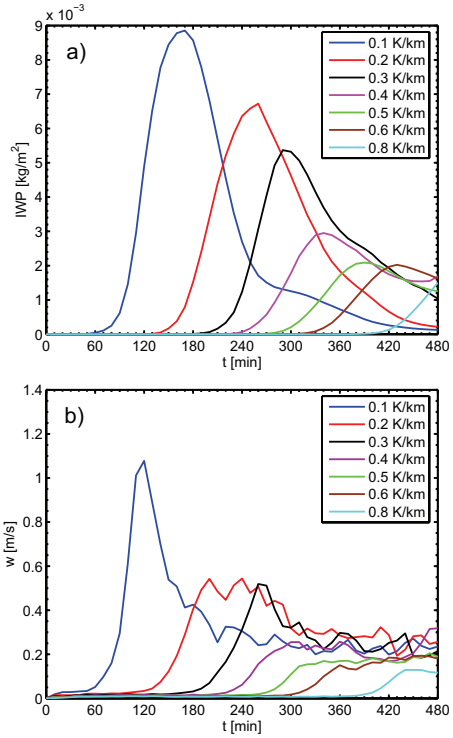

Fig. 6. (a) $\overline{\text{IWP}}$ (averaged over all columns) for thermal stratification $\partial\theta/\partial z$=0.1 to 0.8 K/km. The purple line represents the reference case; **(b)** median of the maximum 5% wind speeds within the ISSR for thermal stratification $\partial\theta/\partial z$=0.1 to 0.8 K/km. The purple line represents the reference case.

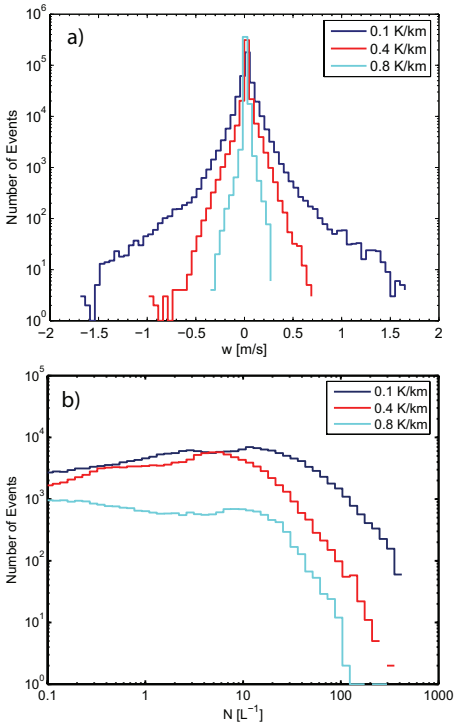

Fig. 7. **(a)** Histogram of vertical velocity for all time steps (for 3 different thermal stratifications $\partial\theta/\partial z$=0.1/0.4/0.8 K/km). The red line represents the reference case; **(b)** histogram of number concentration for all time steps (for 3 different thermal stratifications $\partial\theta/\partial z$=0.1/0.4/0.8 K/km. The red line represents the reference case.)

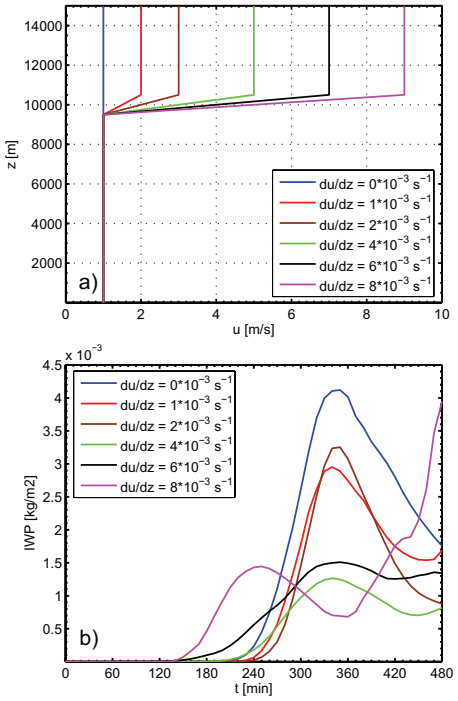

Fig. 8. **(a)** 6 vertical profiles for horizontal wind speed containing different wind shears within the ISSR. The red line represents the reference case; **(b)** $\overline{\text{IWP}}$ (averaged over all columns) for windshears from 0 to 8×10^{-3} s^{-1}.

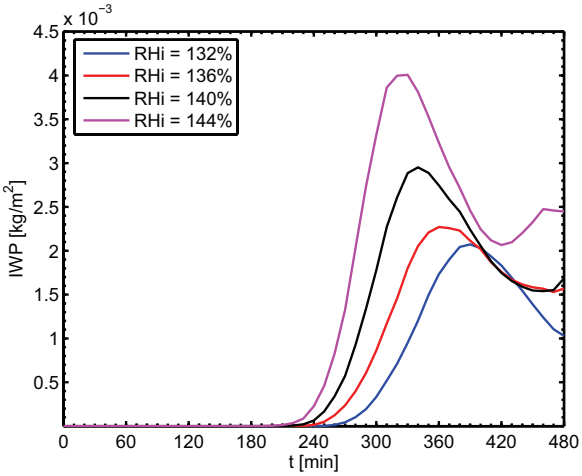

Fig. 9. Mean ice water path $\overline{\text{IWP}}$ (averaged over all columns) of simulations using different initial values for RHi inside the ISSR (RHi=132 to 144%). The black line represents the reference case.

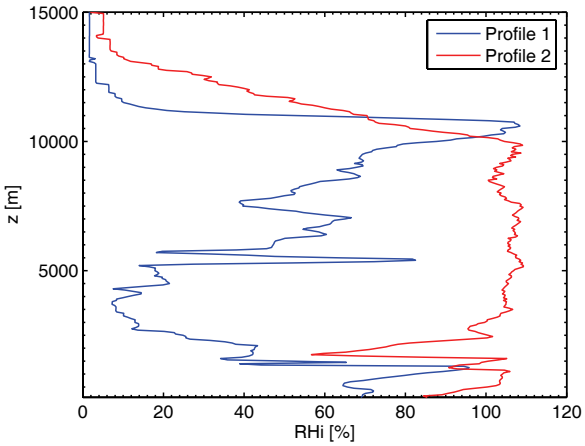

Fig. 10. Profile 1: steep upper RHi gradient (Lindenberg 1 July 2000 06:00 UTC); Profile 2: weak upper RHi gradient (Lindenberg 4 March 2001 06:00 UTC).

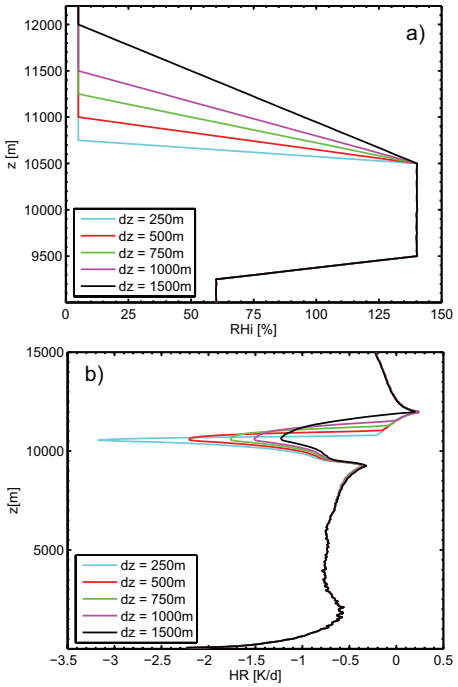

Fig. 11. (a) Vertical RHi profiles of ISSRs using different upper gradients; **(b)** radiative heating rates for 5 different RHi gradients (initial conditions, see a).

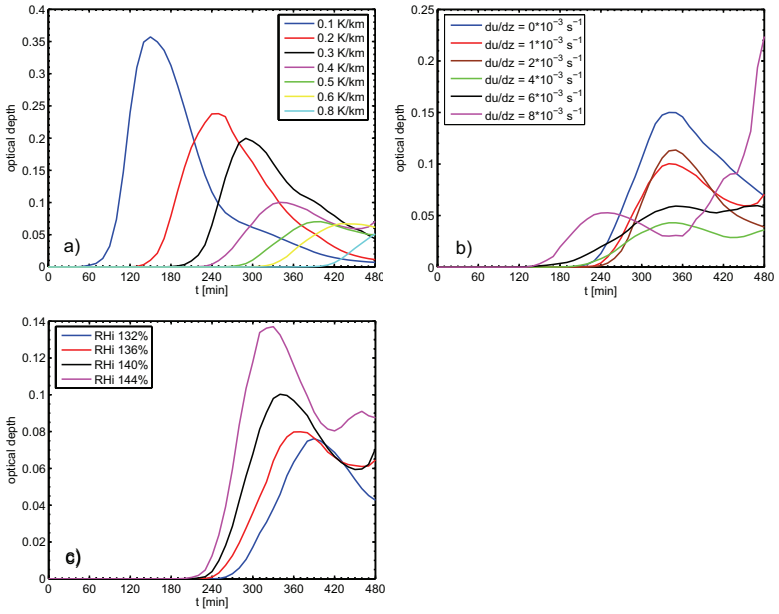

Fig. 12. Mean optical depth (as a function of time) of cirrus clouds, triggered by radiative cooling for following sensitivity studies: **(a)** thermal stratification; **(b)** dynamic stability (variation of vertical wind shear); **(c)** RHi, using different peak values inside the ISSR.

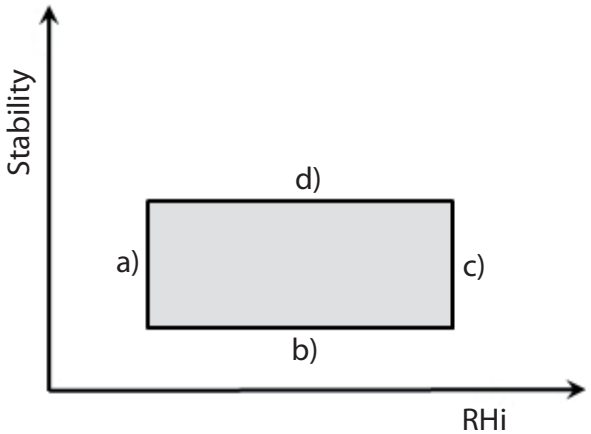

Fig. 13. Phase-diagram of possible conditions, for which thermal emission is an important cloud-building factor in dependence of the stability (statical and dynamical) and the RHi within an ISSR. The regions outside b) and c) accord to spontaneous cloud formation without an influence of radiation, whereas outside a) and d) the conditions supress any cloud formation within the simulation time.